Tissue immunology and leukocyte trafficking

Basic

Research Article

A fluorescent reporter model for the visualization and characterization of T_{DC}

Alessandra Fiore[1], Eleonora Sala[1], Chiara Laura[1,2], Michela Riba[3],
Maria Nelli[1], Valeria Fumagalli[1,2], Federico Oberrauch[1],
Marta Mangione[1], Claudia Cristofani[1,2], Paolo Provero[3,4],
Matteo Iannacone[1,2,5] 🆔 *and Mirela Kuka[1,2]*

[1] School of Medicine, Vita-Salute San Raffaele University, Milan, Italy
[2] Division of Immunology, Transplantation, and Infectious Diseases, IRCCS San Raffaele Scientific Institute, Milan, Italy
[3] Center for Omics Sciences, IRCCS San Raffaele Scientific Institute, Milan, Italy
[4] Department of Neurosciences "Rita Levi Montalcini", University of Turin, Turin, Italy
[5] Experimental Imaging Centre, IRCCS San Raffaele Scientific Institute, Milan, Italy

T_{DC} are hematopoietic cells that combine dendritic cell (DC) and conventional T-cell markers and functional properties. They were identified in secondary lymphoid organs (SLOs) of naïve mice as cells expressing CD11c, major histocompatibility molecules (MHC)-II, and the T-cell receptor (TCR). Despite thorough characterization, a physiological role for T_{DC} remains to be determined. Unfortunately, using CD11c as a marker for T_{DC} has the caveat of its upregulation on different cells, including T cells, upon activation. Here, we took advantage of Zbtb46-GFP reporter mice to explore the frequency and localization of T_{DC} in different tissues at steady state and upon viral infection. RNA sequencing analysis confirmed that T_{DC} sorted from Zbtb46-GFP mice have a gene signature that is distinct from conventional T cells and DC. In addition, this reporter model allowed for identification of T_{DC} in situ not only in SLOs but also in the liver and lung of naïve mice. Interestingly, we found that T_{DC} numbers in the SLOs increased upon viral infection, suggesting that T_{DC} might play a role during viral infections. In conclusion, we propose a visualization strategy that might shed light on the physiological role of T_{DC} in several pathological contexts, including infection and cancer.

🖥 Additional supporting information may be found online in the Supporting Information section at the end of the article.

Introduction

T_{DC} are hematopoietic cells that combine dendritic cell (DC) and conventional T-cell markers and functional properties. They were

identified by Kuka et al. in the SLOs of naïve mice as cells expressing CD11c and MHC-II, two molecules used to identify murine DC, as well as TCRβ, a defining marker for conventional T cells [1, 2]. From an ontogenic point of view, T_{DC} are thymus derived since they were not detected in the spleens of athymic mice and they require the same thymic positive selection as conventional T cells. They are positive for other T-cell markers, such as CD3,

Correspondence: Dr. Mirela Kuka
e-mail: kuka.mirela@hsr.it

Thy-1, and CD27, express CD4 or CD8β at the same ratio as conventional T cells, and present a polyclonal Vβ repertoire comparable to conventional αβ T cells. At steady state, T_{DC} do not display signs of recent activation (CD69, CD25, or IL-7Rhi) or T-cell memory markers, excluding the hypothesis that T_{DC} might represent a subset of activated conventional T cells. In addition, this population does not express other lineage markers, excluding that they might belong to other innate cell subsets such as pDC, NK, or NKT [1].

DC are innate cells that bridge innate and adaptive immunity, given their key role in T-cell activation. They rely on the expression of MHC molecules and costimulatory ligands for their antigen-presenting and T-cell priming activities [3]. T_{DC} resemble DC in their capacity to expand after FLT3L-mediated stimulation and in the ability to respond to TLR agonists such as LPS. Notably, after TLR stimulation, T_{DC} release IL-12, a cytokine normally produced by DC and important for Th1 polarization. T_{DC} also express CD80/CD86 and in vitro studies showed that they can present antigen to $CD4^+$ T through MHC-II [1]. On the other hand, the TCR expressed by T_{DC} is functional and it can be triggered in vitro both by monoclonal antibodies directed to CD3 and by cognate antigens. These experiments also led to the intriguing hypothesis that T_{DC} might be self-sufficient in antigen presentation since they can potentially provide co-stimulation to themselves [1]. Finally, T_{DC} were found also in humans: approximately 0.2% of peripheral blood lymphocytes (PBLs) are $CD3^+$ $TCR\alpha\beta^+$ $CD11c^+$ and $HLA-DR^+$ (MHC-II) [1].

These features render T_{DC} the first unconventional polyclonal T-cell subset that has ever been described and potentially key in the context of immune responses. Unfortunately, using CD11c as a marker for T_{DC} has the caveat of its upregulation on some T-cell populations upon activation [4–7], thus leading to potentially confounding gating strategies. Since, positivity for CD11c can be used for the identification of T_{DC} in steady-state conditions but not in inflammation or other pathological settings, a more specific marker is needed to further investigate T_{DC} functions in peripheral organs or during inflammation.

Since T_{DC} appear to be developmentally related to both conventional T cells (they need a thymus for development) and classical DC (they express FLT3 and expand upon FLT3L-mediated stimulation), we asked whether we could rely on the DC-restricted transcription factor Zbtb46 to identify T_{DC} in settings of inflammation and infection [8]. Indeed, Zbtb46 is expressed by all subsets of conventional myeloid DCs, including their direct precursors in the BM [8, 9]. Microarray and qPCR analysis revealed that Zbtb46 was also expressed by T_{DC}, indicating that they might derive by the same precursors as classical DC [1]. Here, we exploited the Zbtb46-GFP reporter mouse model to explore the frequency and localization of T_{DC} in peripheral tissues such as the liver, small intestine, and lung. RNA sequencing analysis confirmed that T_{DC} identified with this reporter model have a gene signature that is distinct from conventional T cells and DC. In addition, frequency and total numbers of T_{DC} in SLOs recapitulated those previously found using CD11c. The Zbtb46-GFP reporter model allowed for the identification of T_{DC} in situ not only in SLOs but also in the liver and lung of naïve mice.

Results

Zbtb46 is a reliable marker for the identification of T_{DC}

We took advantage of Zbtb46-GFP knock-in reporter mice, which express GFP in all cells with an activated Zbtb46 promoter [8]. Despite being a DC-specific marker, it was reported that Zbtb46 expression was not required for DC development [10]. Therefore, since both heterozygous and homozygous mice can be used to track cells of DC lineage, we decided to use only homozygous mice for a more efficient detection of the GFP fluorescence.

First, spleens and lymph nodes (LNs) of naïve Zbtb46-GFP mice were analyzed and characterized in order to validate this fluorescent reporter model. We found that the frequency of classical DC ($CD11c^+MHC-II^+$) and T_{DC} ($CD11c^+MHC-II^+TCR\beta^+$) in reporter mice was comparable to WT mice, confirming that lack of *Zbtb46* does not affect DC development and recruitment to SLOs (Fig. 1A). To understand whether Zbtb46 expression can be used in place of CD11c to identify DC and T_{DC}, we gated DC using both markers. We found that although about 70–75% of $CD11c^+MHC-II^+$ cells expressed GFP (Fig. 1B), more than 98% of the GFP^+MHCII^+ population was CD11c-positive. These findings indicate that Zbtb46 expression is highly specific and can be used as a valid marker in substitution of CD11c. We then analyzed the percentage of T_{DC}, defined as cells positive for the $TCR\beta$ chain within the population of $GFP^+MHC-II^+$ cells (Fig. 1C and Supporting information Fig. S1A). Frequency and total numbers of T_{DC} in spleens of Zbtb46-GFP mice recapitulated those found using CD11c as a marker, thus confirming the validity of our model (Fig. 1D). The mean fluorescence intensity (MFI) of GFP was slightly but consistently lower in T_{DC} with respect to DC (Supporting information Fig. S1C). Of note, dimensions and granularity of T_{DC} were comparable to those of classical DC, as indicated by the analysis of physical parameters such as forward scatter area (left) and side scatter area (Supporting information Fig. S1B). This observation rules out the possibility that T_{DC} might represent T-DC doublets, a hypothesis that was already thoroughly addressed and excluded in the original report on this new cell population [1].

T_{DC} are distinct from conventional T cells and DC with regard to their transcriptional profile and surface markers

To investigate the gene expression profile of T_{DC}, we performed a bulk RNA sequencing (RNAseq) on T_{DC} from Zbtb46-GFP reporter mice. T_{DC} were sorted from splenocytes of naïve mice along with conventional T cells and DC. The sorting protocol which had been
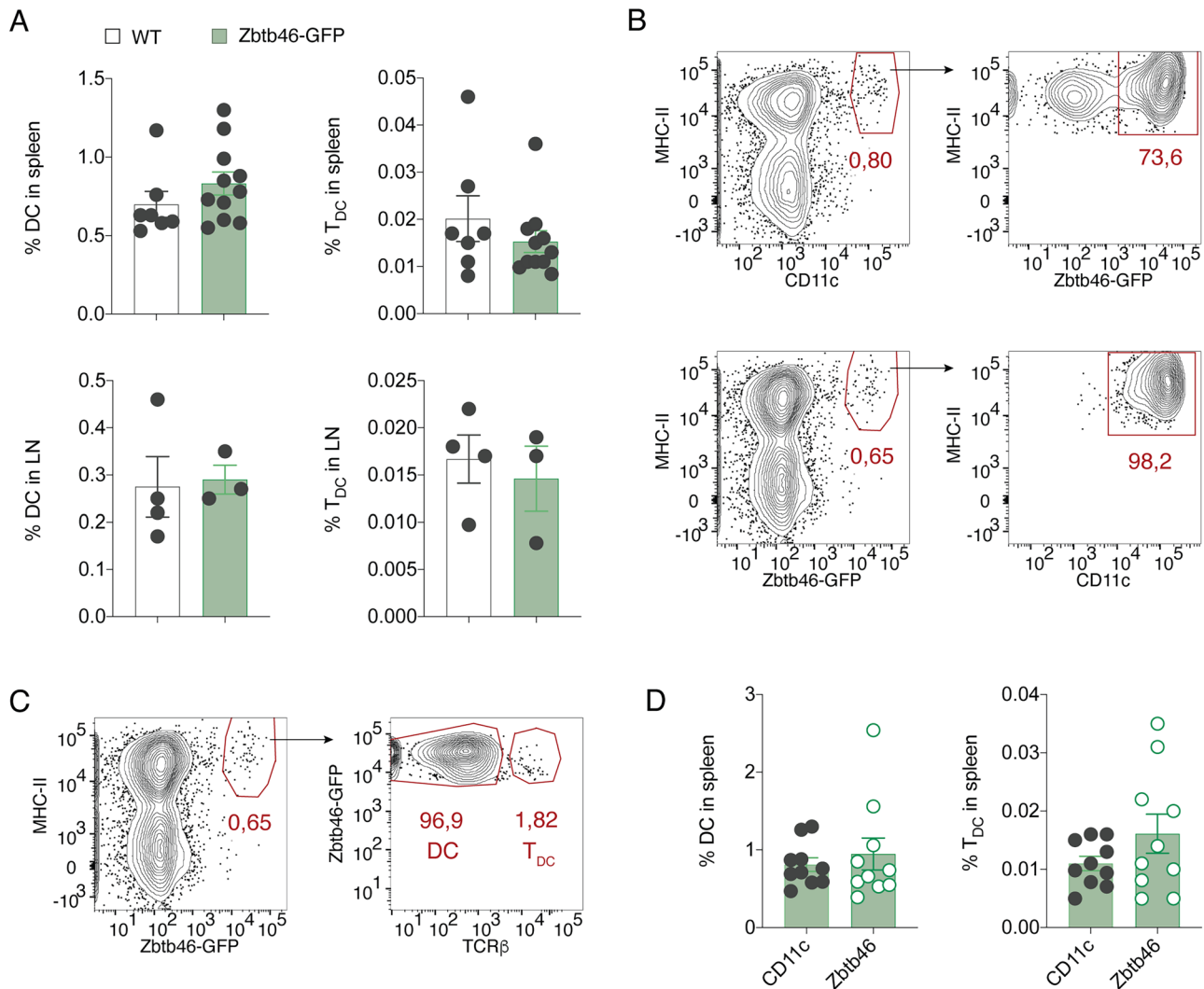
Figure 1. Zbtb46 is a valid substitute of CD11c marker for the identification of T_{DC}. (A) Spleens and popliteal LNs from naive WT or homozygous Zbtb46-GFP mice were collected and stained for the typical DC markers, CD11c and MHC-II (I-Ab). Frequencies of DC (left) and T_{DC} (right) in spleens and LNs are shown. *n* = 7 (WT spleen), 11 (Zbtb46-GFP spleen), 4 (WT LN), 3 (Zbtb46-GFP LN). Mean ± SEM is shown. Data were pooled from two to three independent experiments. Statistics is not shown since there are no statistically significant differences between conditions. (B) Representative plots showing the frequency of GFP+ cells within the CD11c+ MHC-II+ population (upper panels) or, conversely, plots showing CD11c expression on GFP+ MHC-II+ cells (lower panels). (C) Representative plot showing the frequency of DC and T_{DC} within the GFP+ MHC-II+ population in the spleen of naïve Zbtb46-GFP mice. (D) Frequencies of DC and T_{DC} gated based on either CD11c or Zbtb46-GFP markers in spleens of naïve homozygous Zbtb46-GFP mice are shown. *n* = 10. Mean ± SEM is shown. Data were pooled from four independent experiments. Statistics is not shown since there are no statistically significant differences between conditions.

previously optimized for this cell type [2] yielded almost 100% pure cells (Fig. 2A and Supporting information Fig. S2).

Principal component analysis showed that cell identity corresponds to the source of the largest variance in the samples (obtained from three independent experiments) analyzed. This variance is not associated to other characteristics of the set of samples or batch effects (Fig. 2B). In addition, hierarchical clustering confirmed a distinct identity of the three cell types, suggesting however a closer relationship between DC and T_{DC} (Supporting information Fig. S3A). These data confirm our previous findings that T_{DC} are characterized by a specific cell identity, distinct from conventional T cells and DC [1]. Note that 2985 genes

were expressed by T_{DC} at higher levels than on conventional T cells (Fig. 2C). Among these genes, we first selected the top 100 differentially expressed genes by T_{DC} with respect to conventional T cells (Fig. 2D). Some of these genes were expressed by both T_{DC} and DC and this strongly suggests that T_{DC} signature in part resembles that of classical DC. We further confirmed this by performing a network analysis on genes that were (1) differentially expressed by T_{DC} versus T cells, (2) expressed at least 50 counts per gene in T_{DC}, and (3) annotated as Zbtb46 neighbors in the STRING protein–protein interaction network database (Supporting information Fig. S3B) [11]. Many genes known to be expressed by the DC lineage (i.e., *Flt3, Spi1, Itgax, Sirpa, Irf8,*
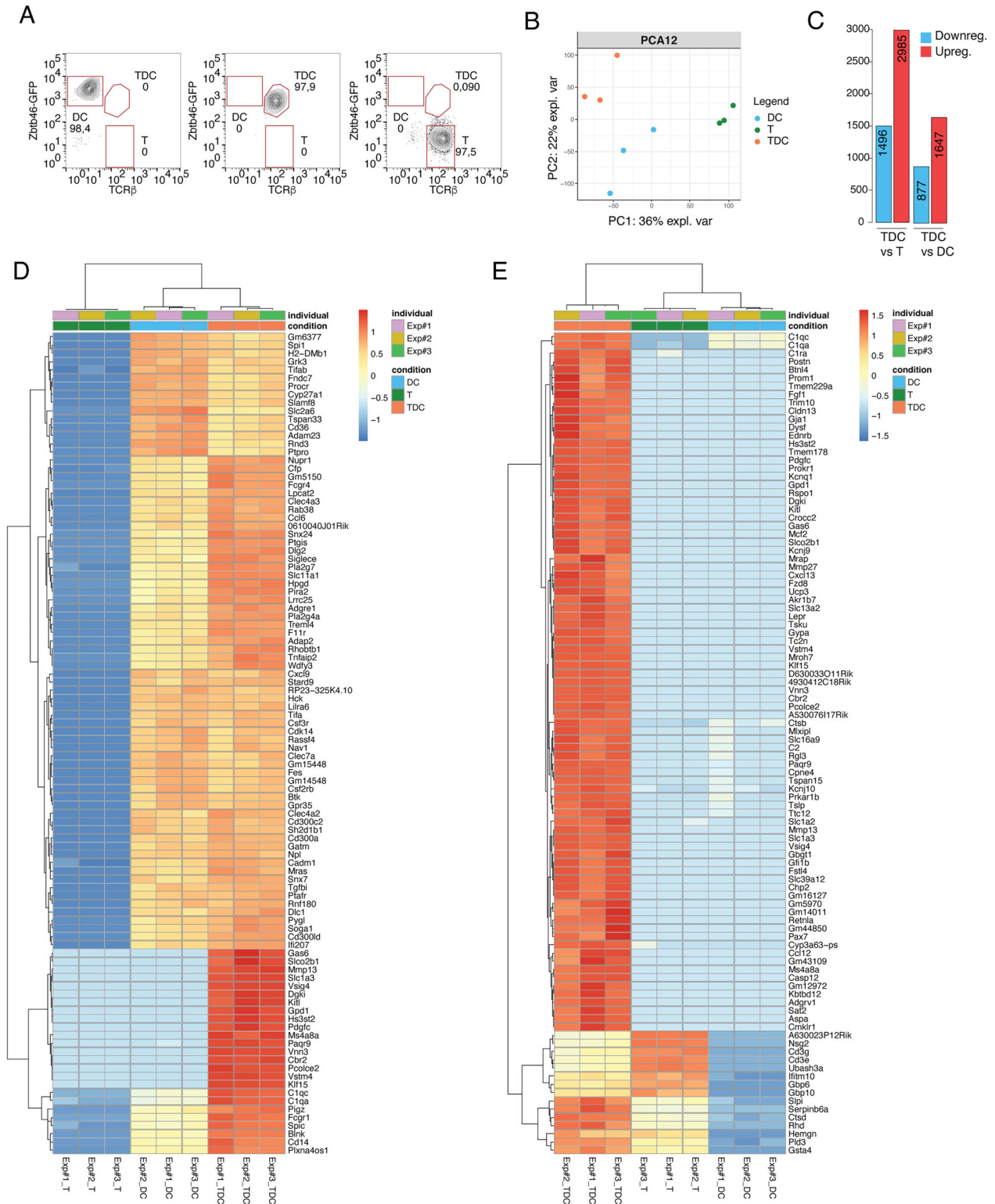
Figure 2. T_{DC} are distinct from conventional T cells and DC with regard to their transcriptional profile. (A) Splenocytes from five naïve homozygous Zbtb46-GFP mice (for each independent experiment) were pooled and DC, T cells, and T_{DC} were sorted. A representative plot of the sorting purity for each cell type is shown. (B) Representation of the first two components of principal component analysis (PCA) accounting for the largest variance in the dataset showing separation of samples according to cell type. (C) Bar plot showing the number of downregulated (blue) and upregulated (red) genes in the indicated comparisons and according to the following cut-off: nominal *p*-value < 0.01 and |log2fold change| > 1. (D) Heatmap showing the top 100 differentially expressed genes in T_{DC} versus T cells. Values in log2(RPKM) were scaled by row across samples. (E) Heatmap showing the top 100 differentially expressed genes in T_{DC} versus DC. Values in log2(RPKM) were scaled by row across samples.

Batf3, and *Csf1r*) were found in this network [12–14]. Please note that Zbtb46 itself is not expressed because cells were sorted from homozygous Zbtb46-GFP mice (Supporting information Fig. S3B). 1647 genes were expressed at significantly higher levels in T_{DC} with respect to DC (Fig. 2C). By performing a Gene Set Enrichment Analysis [15], we found that the T-cell signature extracted from the Panglao database [16] is significantly enriched with some of these genes (Supporting information Fig. S3C). We then proceeded in selecting the top 100 differentially expressed genes by T_{DC} with respect to classical splenic DC (Fig. 2E). Most of the genes shown in the heatmap of Fig. 2E are specifically expressed by T_{DC} with respect to both conventional T cells and DC, whereas some of them are shared with T cells. Finally, we asked whether T_{DC} sorted from Zbtb46-GFP reporter mice express typical cytotoxic genes, as previously reported for T_{DC} identified via CD11c [1]. Although with a high degree of variability among biological replicates, genes like *Gzmb, Gzma, Nkg7, Prf1*, and *Ifng* were expressed at higher levels by T_{DC} with respect to DC (Supporting information Fig. S3D). Overall, these data confirm that T_{DC} identified with the Zbtb46-GFP reporter mouse are distinct from both conventional T cells as well as DCs.

We further employed flow cytometry to analyze several surface markers expressed by T_{DC} with respect to other cell types. Besides Zbtb46-GFP, CD11c and MHC-II were also expressed by both DC and T_{DC} (although this latter cell type express them at lower levels with respect to DC) but not by T cells and monocytes (identified as $CD11b^+Ly6C^+Ly6G^-$ cells in naïve spleens) (Supporting information Fig. S4A). TCRβ and CD3 were instead expressed at similar levels in T cells and T_{DC}, but not in DC and monocytes (Supporting information Fig. S4A). Finally, as previously shown in the original paper [1] T_{DC} express both CD44 (like DC and monocytes) and CD62L (like naïve T cells) and thus do not seem to represent an activated T-cell subset (Supporting information Fig. S4A).

Since RNA sequencing data revealed that monocyte/macrophage-related genes were among the highest differentially expressed genes by T_{DC} (Fig. 2E), we sought to analyze protein levels of some of these markers in T_{DC} compared with monocytes. We found that CD11b, Ly6C, CD64, and Clec9a were expressed at significantly higher levels in monocytes with respect to T_{DC} and DC, and that their expression on T_{DC} was similar (CD64 and Clec9a) if not lower (CD11b) with respect to classical DC, indicating that T_{DC} definitively resemble more the DC than the monocyte lineage (Supporting information Fig. S4B). Finally, T_{DC} do not express CD19, Ly6G, and NKp46, defining markers of B cells, neutrophils, and NK cells, respectively; however, they do express slightly higher levels of GzmB and the degranulation marker CD107 with respect to T and NK cells (Supporting information Fig. S4C).
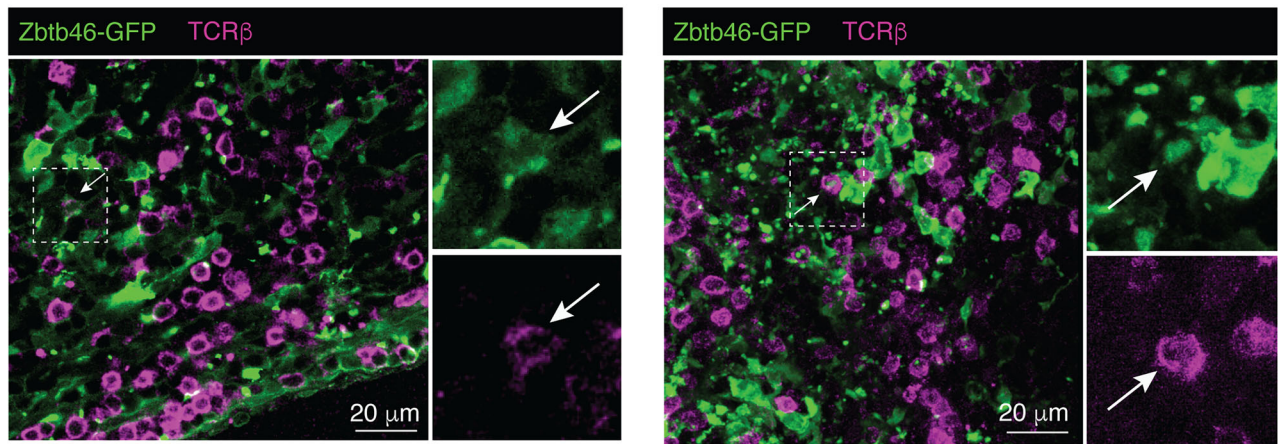
T_{DC} can be identified in situ in SLOs and peripheral organs of naïve Zbtb46-GFP BM chimeras

We asked if we could identify T_{DC} in situ in SLOs from naïve mice by using the Zbtb46-GFP reporter. Although the original paper describing the Zbtb46-GFP mouse model reported GFP expression in a small fraction of endothelial cells [8], we found a much higher expression than expected at the point that we could not distinguish DC from stromal cells in SLOs (Supporting information Fig. S5A and B). Indeed, most of the GFP signal was located close to the LN subcapsular sinus (denoted by the CD169 staining) and outside the splenic white pulp (also denoted by the CD169 staining), respectively, instead of being localized to the LN paracortex or to the white pulp where DC reside [3]. Therefore, we decided to generate BM chimeras to restrict GFP expression to the hematopoietic compartment. This allowed for the GFP signal to be detected exclusively in DCs and localized to the LN paracortex and to the splenic white pulp (Supporting information Fig. S5C and D). We then looked for T_{DC} in situ by staining sections from Zbtb46-GFP BM chimeras with an anti-TCRβ antibody. Confocal microscopy in LN sections revealed rare cells positive for GFP and TCRβ concomitantly (Fig. 3A). These cells were frequently located in interfollicular areas, close to B-cell follicles or to the subcapsular sinus (Supporting information Fig. S6A). Similar cells were also detected in the white pulp of spleens from naïve reporter BM chimeras (Fig. 3B and Supporting information Fig. S6B). Interestingly, confocal imaging of a granzyme B (Gzmb)-tdTomato fluorescent reporter model (for validation of the model please refer to [17] and Supporting information Fig. S7) showed that some $GFP^+ TCRβ^+$ cells also expressed GzmB (Fig. 3C), in line with previously published data showing T_{DC} as having a cytotoxic profile [1]. However, due to the very low frequency of GzmB positivity among $GFP^+TCRβ^+$ cells, we decided to continue our characterization of T_{DC} with the Zbtb46-GFP reporter only, combined with TCRβ staining.

Like other innate lymphocytes or lymphoid cells, T_{DC} might locate not only to SLOs but also to peripheral tissues, so that they can respond to infections in a prompt way. We decided to exploit the Zbtb46-GFP reporter model to explore the presence of T_{DC} in peripheral tissues often in contact with pathogens. We started with the lung, since this is a very important infection site for all respiratory viruses [18]. Confocal imaging of perfused lung sections contained rare cells expressing both GFP and TCRβ, suggesting that the lung might be a localization site of T_{DC} at steady state (Fig. 4A). Flow cytometry analysis showed that the frequency of T_{DC} in the lungs was comparable to that of the spleens of the same animals (Fig. 4C). Next, we looked at the liver, which is in contact with many antigens derived from the gut as well as being an infection site for both hepatotropic and systemic viruses [19–21]. Cells expressing GFP and TCRβ were identified in the parenchyma of perfused livers from naïve mice (Fig. 4B); interestingly, the frequency of T_{DC} (detected by flow cytometry) among intrahepatic leucocytes was significantly higher than in the spleens of the same mice (Fig. 4D). These findings indicate that the liver might be a preferential location site for T_{DC}. By contrast, we found a very low frequency of Zbtb46-positive cells in the small intestine, and they were almost all DC, with very few and almost undetectable T_{DC}, suggesting that this organ might not be populated by T_{DC} at steady-state conditions (Fig. 4E).
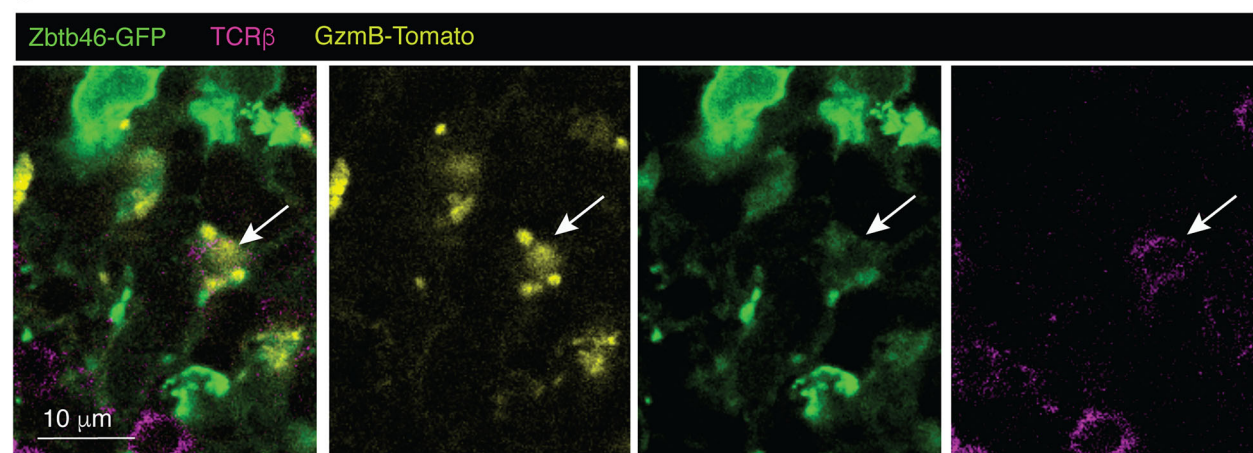
## A Popliteal LNs of naive mice
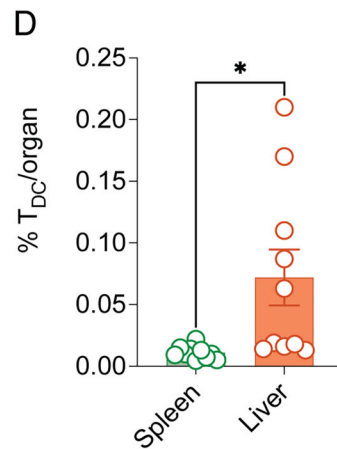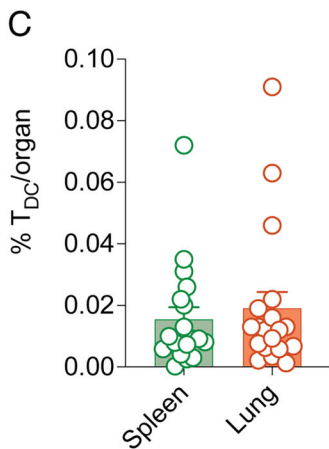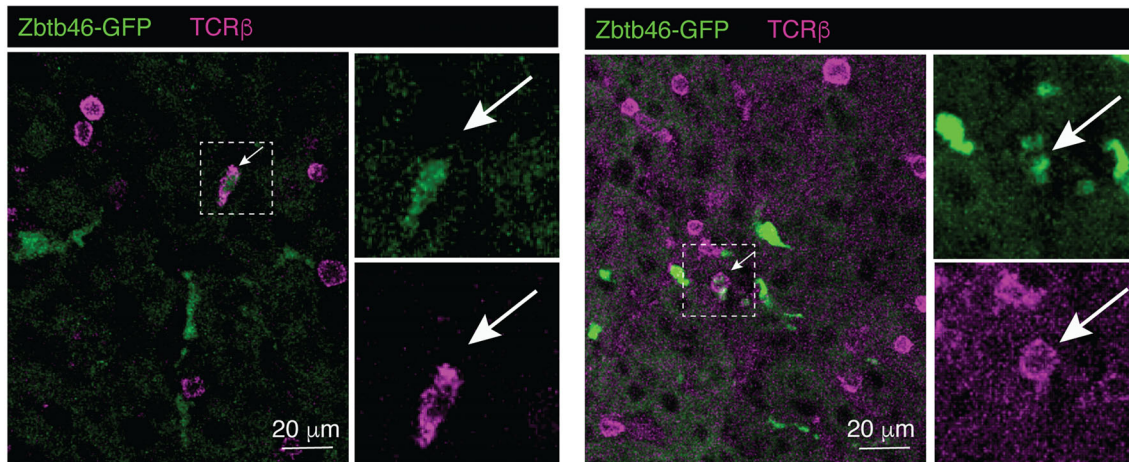

B Spleens of naive mice
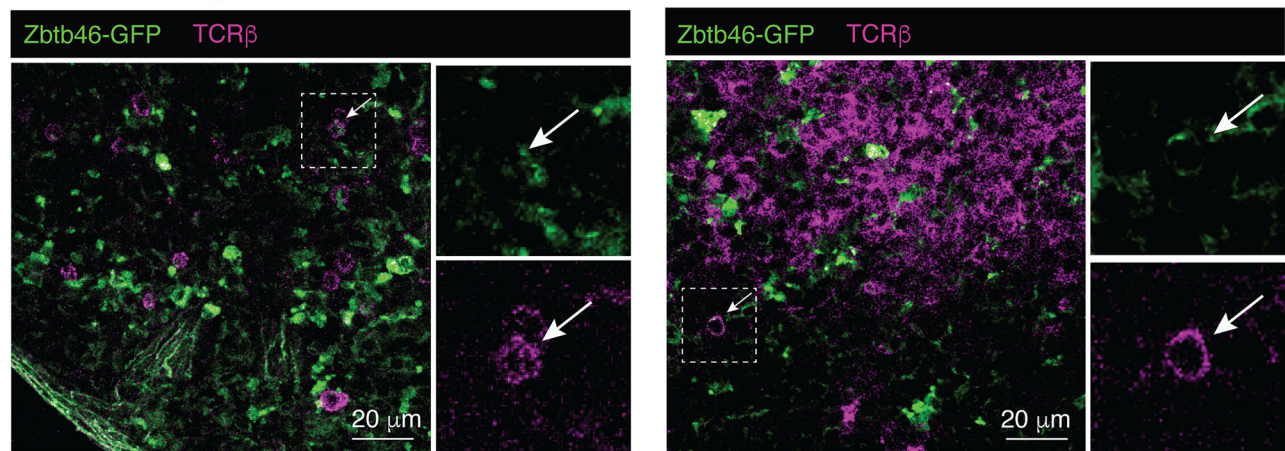
C

Figure 3. T_{DC} can be identified in situ in SLOs of naïve Zbtb46-reporter BM chimeras. LNs (A) and spleens (B) from naive homozygous Zbtb46-GFP BM chimeras were analyzed by confocal microscopy. Confocal micrographs of two representative mice are shown. Scale bars represent 20 μm. Zbtb46-GFP$^+$ cells are in green, and TCRβ$^+$ cells are in purple. Cells that express both markers concomitantly are indicated with an arrow, and magnification is shown on the right. (C) A representative confocal micrograph of a naïve LN (one of the two LNs depicted in A) showing a cell that expresses concomitantly Zbtb46-GFP, TCRβ, and GzmB-Tomato. The scale bar represents 10 μm.
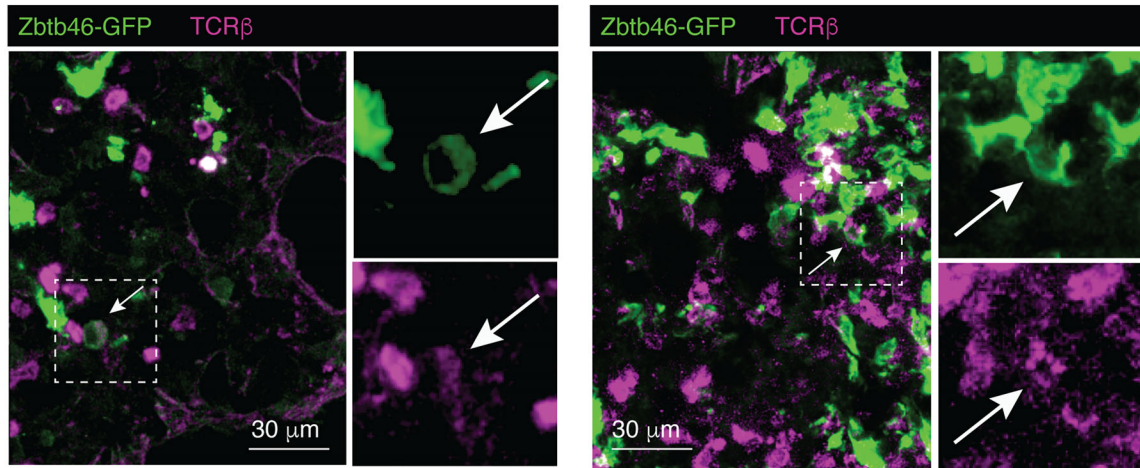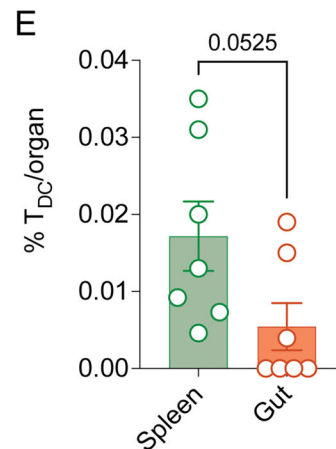
Figure 4. T_{DC} can be identified in lungs and livers of naïve Zbtb46-reporter mice. Lungs (A) and livers (B) from naive homozygous Zbtb46-GFP BM chimeras were analyzed by confocal microscopy. Confocal micrographs of two representative mice are shown. Scale bars represent 30 μm (A) and 20 μm (B). Zbtb46-GFP$^+$ cells are in green, and TCRβ$^+$ cells are in purple. Cells that express both markers concomitantly are indicated with an arrow, and magnification is shown on the right. Frequencies of T_{DC} in lungs (C), livers (D), and gut (E) of naïve homozygous Zbtb46-GFP mice analyzed by flow cytometry are shown. $n = 19$ (spleen vs. lung), $n = 10$ (spleen vs. liver), $n = 6$ (spleen vs. gut). Mean ± SEM is shown. Data were pooled from four independent experiments (lung and liver) or from two independent experiments (gut); *p value < 0.05.

Viral infection leads to enrichment of T_{DC} in the SLOs

We previously showed that adoptively transferred Ag-specific T_{DC} could expand in response to systemic infection with lymphocytic choriomeningitis virus (LCMV) [1]. However, because CD11c is upregulated on some T-cell populations during immune activation [4–7], it is difficult to establish whether numbers and frequencies of endogenous T_{DC} change during viral infection. In particular with regard to LCMV infection, the gating strategy based on CD11c and MHC-II double positive cells is not ideal for T_{DC} identification, since at day 7 post-infection the frequency of CD11c$^+$MHC-II$^+$ cells is substantially increased (Supporting information Fig. S8A) mainly due to the fact that the majority of TCRβ$^+$ cells acquire CD11c expression (Supporting information Fig. S8B). Importantly, Zbtb46 expression profile did not change upon LCMV infection (Supporting information Fig. S8C and D) and thus the Zbtb46-GFP reporter represents an ideal model to investigate whether T_{DC} expand in LCMV-infected mice. LCMV infection resulted in a significant increase in the frequency of both T_{DC} and conventional T cells in the spleens of LCMV-infected mice analyzed 7 days after infection (Fig. 5A). This effect was specific to these two cell types, as frequencies of classical DC did not change significantly (if anything they were found in lower frequency in LCMV-infected mice) (Fig. 5A). Mice infected subcutaneously (s.c.) in the footpad showed a slightly different trend (Fig. 5B): although a higher frequency of DC was found in the draining LNs 7 days postinfection (Fig. 5B), the frequency of total T cells and total T_{DC} did not increase like in the spleen (Supporting information Fig. S9). We reasoned that, since LCMV is known to strongly expand CD8$^+$ T cells, the total number of T cells upon s.c. infection might reflect the aftermath of a high increase in the CD8 T-cell compartment and a relative decrease in the CD4 T-cell compartment. Indeed, when we analyzed only CD8$^+$ T cells and CD8$^+$T$_{DC}$, we could appreciate a substantial increase in both cell populations upon infection (Fig. 5B). Confocal imaging of LN sections from infected mice presented quite a few cells positive for both GFP and TCRβ, thus confirming an enrichment of T_{DC} in these organs upon infection (Fig. 5C and D). Taken together, these results indicate that T_{DC} expands in SLOs in response to LCMV infection.

Since T_{DC} represent a population of T cells with innate traits, we asked whether T_{DC} might start expanding earlier than conventional T cells upon infection. Two days upon systemic LCMV, the frequency of T_{DC} in the spleens of infected mice was higher than in uninfected controls, although the difference was not statistically significant (Supporting information Fig. S10A). A similar trend was observed for CD8$^+$ T_{DC} in the draining LNs of subcutaneously infected mice, whereas no changes were observed in total T_{DC} (Supporting information Fig. S10B and C). The frequency of conventional T cells and DC did not increase at this timepoint, suggesting a specific and distinct dynamics for T_{DC} that requires further investigation. Moreover, we found that the levels of the cytotoxic markers GzmA and GzmB, and of the degranulation marker CD107, were significantly increased in splenic T_{DC} 2 days upon LCMV infection (Supporting information Fig. S11A–C). On the contrary, TCRβ levels were slightly downregulated (Supporting information Fig. S11C), which is in line with the engagement of the TCR during this activation process. All in all, these data suggest that T_{DC} might be engaged by the antigen and perform their cytotoxic functions very early upon infection, although these data should be corroborated by more in depth analysis.

The transcriptional profile of T_{DC} overlaps with a subset of T cells found in the gut during bacterial infection

Recently, a new subset of CD4$^+$ T cells was identified in the gut of mice infected with *Salmonella* [22]. These cells were named MyT since they express both T-cell markers and myeloid-cell markers. We asked whether MyT and T_{DC} might represent the same cell type, and to test this hypothesis we decided to compare these two populations at the transcriptomic level. First, we re-analyzed the published scRNAseq dataset reporting the existence of MyT [22], focusing on T_{eff} cells only as the authors did. We performed dimensionality reduction on t-distributed stochastic neighbor embedding plot, highlighting the pathogen used to infect the mice (Fig. 6A). Then, MyT cells were identified among the cells belonging to the *Salmonella* infection condition (Fig. 6B). This annotation was based on the expression of both myeloid cell markers (*H2-Ab1*, *C1qa*, *Lyz2*, *Apoe*) and T-cell markers (*Cd3d* and *Trac*), as previously reported [22] and as shown in Supporting information Fig. S12. A doublet detection analysis performed with the DoubletFinder tool [23] excluded the presence of doublets among MyT and any other cluster of the analyzed dataset (Supporting information Fig. S13). We then compared the transcriptome of MyT cells with the one of T_{DC} obtained from the bulk RNA sequencing experiment previously performed (Fig. 2). To this end, we built a T_{DC} signature using the top 100 differentially expressed genes by T_{DC} with respect to conventional T cells in the bulk RNA sequencing experiment (Fig. 2D). We observed a significant enrichment of this signature in the MyT population compared to the other T cells (Fig. 6C and D). Moreover, the genes belonging to the previously published T_{DC} signature obtained as the ones upregulated in T_{DC} versus T cells [1] are also highly expressed by the MyT population (Supporting information Fig. S14). Overall, these data strongly suggest that T_{DC} and MyT might represent similar if not identical cell populations.

Discussion

T_{DC} are unconventional polyclonal T cells that combine innate and adaptive cell properties. When triggered in vitro, they can respond either as DC or as conventional T cells depending on the stimulus [1]. However, these represent only potential functional properties of T_{DC} and there is no formal proof that their behavior in vivo is similar. In general, the physiological role and relevance of T_{DC} in vivo is unknown. The main reason for this is a technical challenge in precisely identifying them due to the low
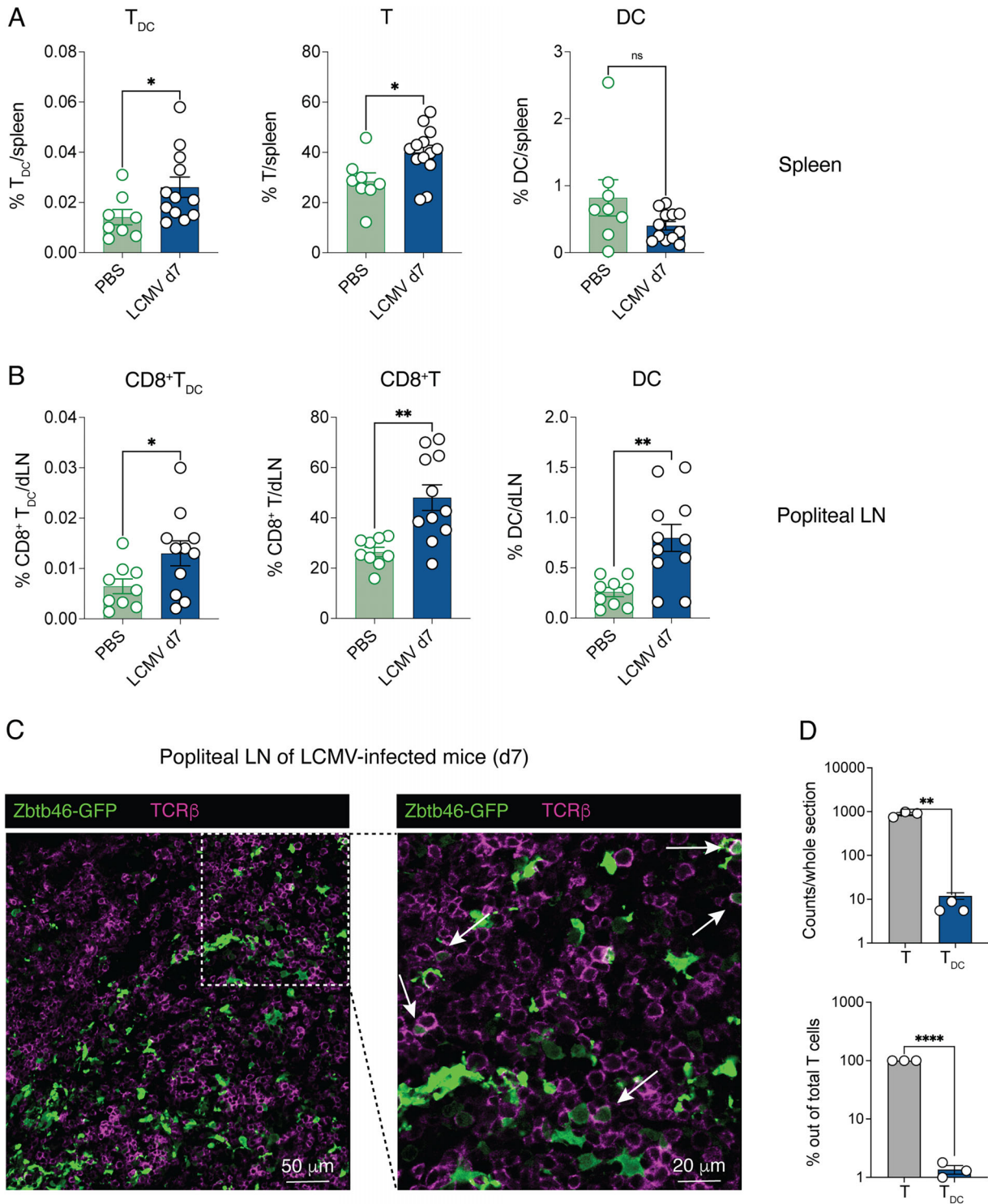
Figure 5. Viral infection leads to enrichment of T_{DC} in the SLOs. Homozygous Zbtb46-GFP mice (A and B) or BM chimeras (C) were infected i.v. or s.c. with LCMV Arm, and SLOs were analyzed 7 days upon infection. (A) Frequencies of total T_{DC}, conventional T cells, and DC in the spleens of i.v. infected mice are shown. $n = 8$ (PBS), $n = 12$ (LCMV). Mean ± SEM is shown. Data were pooled from four independent experiments. *p value < 0.05. (B) Frequencies of $CD8^+ T_{DC}$, $CD8^+$ T cells, and total DC in the draining LNs (dLNs) of s.c. infected mice are shown. $n = 9$ (PBS), $n = 11$ (LCMV). Mean ± SEM is shown. Data were pooled from three independent experiments. *p value < 0.05, **p value < 0.01. (C) dLNs from LCMV-infected Zbtb46-GFP BM chimeras were analyzed by confocal microscopy 7 days upon infection. Confocal micrographs of a representative section and a magnification (dotted square) are shown. Scale bars represent 50 µm (whole section) and 20 µm (magnification). Zbtb46-GFP⁺ cells are in green, and TCRβ⁺ cells are in purple. Cells that express both markers concomitantly are indicated with an arrow. (D) Quantification of TCRβ⁺ cells (T cells) and Zbtb46-GFP⁺ TCRβ⁺ (T_{DC}) is shown as counts per each whole section (upper graph) and as frequencies out of total T cells (lower graph). $n = 3$. **p value < 0.01, ****p value < 0.0001.
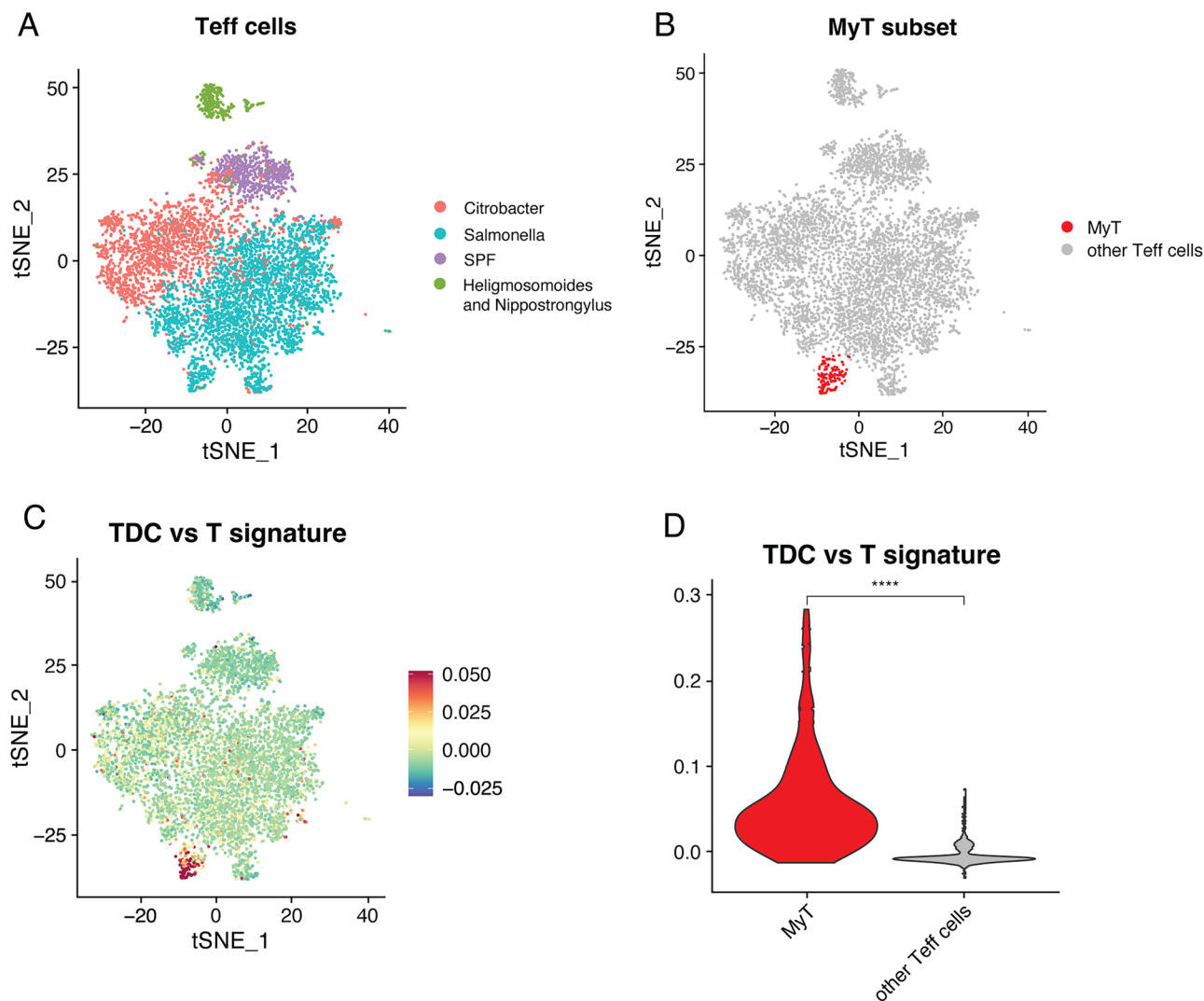
Figure 6. The transcriptional profile of T_{DC} overlaps with that of MyT, a subset of T cells found in the gut during bacterial infection. (A) t-Distributed stochastic neighbor embedding (t-SNE) representation of effector T cells from Kiner et al. Each dot corresponds to a single cell, colored according to the infectious conditions. (B) Highlight of the MyT population in the t-SNE in (A) based on the expression of genes in Supporting information Fig. S8. (C) Feature plot of a T_{DC} signature (top 100 DEGs in the comparison TDC vs. T) obtained from the bulk RNA seq experiment, max.cutoff parameter set to "q95." (D) Violin plot showing the enrichment of the T_{DC} signature in the MyT population compared to the other T cells. ****p value < 0.0001 using a Wilcoxon test.

frequency of these cells and the lack of specific markers that can be exploited to generate T_{DC}-deficient mice. In addition, the combination of markers used to identify T_{DC} in the SLOs of naïve mice are not ideal for their identification in peripheral organs or during inflammation and infection, conditions where the integrin CD11c is widely expressed also in cell types other than the DC lineage [4–7]. Here, we tackle this last caveat by taking advantage of a fluorescent reporter mouse strain already used in the past to identify DC [8–10]. Thanks to this reporter model, we could detect T_{DC} in situ in SLOs, lung, and liver, both at steady state and upon viral infection.

In the SLOs of naïve mice, T_{DC} cells were frequently located in interfollicular areas, close to B cell follicles or to the subcapsular sinus, reminiscent of a previously described innate αβ CD8 T-

cell population previously described by Kastenmuller et al. [24]. These innate αβ CD8 T cells were found to be among the main producers of IFN-γ very early after infection and located to the subcapsular sinus, but were not further characterized. Of note, bulk RNA sequencing showed that T_{DC} of naïve mice are highly enriched in *Ifng* expression (Supporting information Fig. S1D), therefore suggesting that they might overlap with the innate cells described previously [24].

Recently, a subset of intestinal ILC3 expressing Zbtb46 was described [25]. Zbtb46 expressed by ILC3 restrains the inflammatory potential of these cells. Before this report, Zbtb46 was known to be expressed only on cells of the DC lineage and on endothelial cells. These latest findings suggest that Zbtb46 is not a DC-restricted marker but it might be expressed also by cells of

lymphoid origin. Although the prevailing dogma attributes to DC and conventional T cells extremely divergent pathways of differentiation, the identification of genes expressed by both myeloid and lymphoid precursors support a common DC/T ontogeny for T_{DC}. For example, IRF8 has been found to be expressed by both T and DC precursors in human thymus, before their commitment to one of the cell lineages [26]. Notably *Irf8* is among the genes which are differentially expressed by T_{DC} with respect to conventional T cells (Supporting information Fig. S3B).

The Zbtb46-GFP reporter model led to the finding that, at steady state, T_{DC} preferentially locate to the liver and to a lower extent to the lung but are excluded by the small intestine. This finding seems in stark contrast with the observation that MyT, a new subset of T cells with myeloid properties and whose transcriptional profile overlaps with the one of $T_{DC,}$ was discovered in the gut in response to bacterial infection [22]. One explanation for this controversy might be that the gut is not a preferential site of location in steady-state conditions, but T_{DC} or MyT might migrate there in response to the infection from elsewhere (i.e., from SLOs). Moreover, we found that LCMV infection leads to preferential expansion of $CD8^+$ T_{DC}, whereas MyT found during bacterial infection express CD4. We have previously reported that in naïve mice T_{DC} can express either CD4 or CD8. This would suggest that different subsets of T_{DC} might be expanded upon infection, depending on the pathogen. Pathogens that lead to strong CD8 T-cell responses like LCMV might lead to expansion of $CD8^+$ T_{DC}, whereas pathogens that trigger CD4 T-cell responses might lead to expansion of $CD4^+$ T_{DC}.

A recent study shows that the liver is populated by $CD8^+$ T cells with myeloid markers on their surface [27]. The authors showed that these myeloid markers (among which CD14) are acquired by T cells following their activation by myeloid cells and result in functional changes in T-cell function. However, these hybrid $CD8^+$ T cells do not express any RNA related to those myeloid markers. By contrast, both T_{DC} and MyT are characterized by a transcriptional profile that combines both myeloid and T-cell markers, therefore we strongly believe that the hepatic $CD14^+CD8^+$ T cells are different from T_{DC}.

RNA sequencing analysis revealed that monocyte/macrophage-related genes were among the highest differentially expressed genes by T_{DC} with respect to T cells and DC. This finding might raise concerns on the identity of the sorted cells, which might seem very similar to monocytes or macrophages. However, we found that surface expression of some of these markers is significantly lower in T_{DC} compared with monocytes, and it is instead very similar to classical DC. This observation, coupled to expression of DC-specific genes, suggests that T_{DC} are a cell type closely related to the DC lineage.

In conclusion, we believe that the T_{DC} visualization strategy we propose might shed light on the physiological role of T_{DC} in several pathological contexts, including infection and cancer. Indeed, further investigation on the localization of T_{DC} in specific organ sub-compartments and their interactions with other cell types, as well as on their enrichment upon specific conditions, might provide new information that can partially overcome the caveat of

the temporary lack of a specific marker that could be used for more functional studies.

Materials and methods

Mice

Mice were housed under specific pathogen-free conditions and used at 8–10 weeks of age, unless otherwise indicated. All experimental animal procedures were approved by the Institutional Animal Committee of the San Raffaele Scientific Institute.

B6.129S6(C)-Zbtb46tm1.1Kmm/J mice (in the text referred to as Zbtb46-GFP) were purchased from The Jackson Laboratory and were always used as homozygous. C57BL/6 were purchased from Charles River. Gzmb-tdTomato mice were kindly provided by Dr. Claude Boyer [17, 28]. BM chimeras were generated by irradiation of C57BL/6 mice with ~900 rad and reconstitution with the indicated BM; mice were allowed to reconstitute for at least 8 weeks prior to use.

Infections and immunizations

Mice were infected s.c. in the footpad with 1×10^5 focus forming units (ffu) or intravenously (i.v.) with 2×10^5 ffu of LCMV Armstrong (LCMV-Arm). Virus was propagated and quantified as described [29] and diluted in 25 µL of PBS prior to s.c. injection or in 200 µL of PBS prior to i.v. injection. All infectious work was performed in designated Biosafety Level 2 and Biosafety Level 3 workspaces in accordance with institutional guidelines.

Cell isolation and flow cytometry

Single-cell suspensions of spleens and LNs were obtained by mechanical dissection and without any enzymatic tissue digestion procedure as previously described [1]. For lungs analysis, mice were perfused through the right ventricle with PBS. Lung tissue was digested in RPMI 1640 containing 3.2 mg/mL Collagenase IV (Sigma, #C5138) and 25 U/mL DNAse I (Sigma, #D4263) for 30 min at 37°C. Homogenized lungs were passed through 70-µm nylon meshes to obtain a single cell suspension. For liver analysis, mice were perfused through the vena cava with PBS. Liver tissues were disrupt using scissors on 70-µm nylon meshes and were digested in RPMI 1640 containing 0.2 mg/mL Collagenase IV and 5 U/mL DNAse I for 40 min at 37°C. After this, cell suspensions were centrifuged at 300 rpm for 3 min and supernatants were recovered. Small intestine was harvested paying attention to remove fat and Peyer patches. It was cut longitudinally and rinsed with PBS, then it was placed in complete medium (DMEM supplemented with 10% FBS, 1% penicillin plus streptomycin, 1% L-glutamine) with 1 mM DTT (Sigma, # 10197777001) for 10 min at 37°C. The pieces of small intestine were then

transferred in complete medium with 1 mM EDTA for 10 min at 37°C. After that, EDTA buffer was replaced with a fresh one for other 10 min at 37°C. Tissue suspension was placed in fresh medium with 1 mg/mL Collagenase D (Sigma, # 11088858001) and 5 U/mL DNase I for 30 min at 37°C. Homogenized intestine was passed through 70-μm strainer and washed one time with PBS.

Cell suspensions obtained from lung, liver, and intestine processing were resuspended with a solution composed of 36% percoll (Sigma #P4937) and 4% PBS 10x in PBS. After centrifugation for 20 min at 2000 rpm (light acceleration and low brake), cells were isolated and counted. Possibly, the remaining red blood cells were removed with ACK lysis.

All flow cytometry stainings of surface-expressed markers were performed in FACS Buffer containing PBS and 2% FBS at 4°C as described [1, 30]. LIVE/DEAD Fixable Near IR (780) (ThermoFisher Scientific) and Fc receptors blocking anti-CD16/32 antibody (Invitrogen # 14-0161-82) were added to cell pellets prior to staining with fluorochrome-conjugated antibodies. Staining of intracellular molecules was performed using BD Cytofix/Cytoperm and Perm/Wash Buffer kit. Antibodies used included CD4 (RM4-5), TCRβ (H57-597), CD8 (K53-6.7), CD11c (N418), MHCII (AF6-120.1), CD44 (IM7), CD19 (ID3), CD11b (MI/70), Ly6C (HK1.4), CD64 (X54-5/7.1), Ly6G (1A8), Clec9a (7H11), GzmB (GB11), CD3 (145-2C11), Nkp46 (29A1.4), CD62L (W18021D), CD107a (1D4B), GzmA (3G8.5), and Zbtb46 (U4-1374 RUO). Fluorochrome-conjugated Abs were purchased from BioLegend, eBioscience, or BD Pharmingen. Samples were collected on a FACS CANTO (BD Pharmingen) or on the spectral flow analyzer Cytek Aurora (Cytek) and analyzed with FlowJo software (Treestar). We have adhered to the guidelines given in [31] for all flow cytometry stainings and analyses.

Confocal immunofluorescence histology

Confocal microscopy analysis of popliteal LNs, spleens, livers, and lungs was performed as previously described [30, 32]. The following primary Abs were used for staining: rat anti-B220 (RA3-6B2), rabbit anti-GFP (Invitrogen), anti-TCRβ (H57), and anti-CD169 (Ser-4). Images were acquired on an inverted Leica microscope (SP8, Leica Microsystems) with a motorized stage for tiled imaging using a HC PL APO CS2 20X objective (NA 0.75). To minimize fluorophore spectral spill over, we used the Leica sequential laser excitation and detection modality. B-cell follicles were defined based on the B220 staining. Quantification of T cells and T_DC was performed using the Spots tool in Imaris (Bitplane).

Cell sorting and RNA extraction

Splenocytes of naive Zbtb46-GFP mice were processed in order to obtain single cells suspensions and T cells, and DCs and T_DC were sorted on a MoFlo XDP Cell Sorter. Briefly, spleno-

cytes were gated for MHC-II and Zbtb46-GFP in order to identify DCs (MHC-II$^+$Zbtb46-GFP$^+$) and non-DCs (MHC-II$^-$Zbtb46-GFP$^-$). Gating on the non-DC population, T cells were identified and sorted as CD3ε$^+$TCRβ$^+$ cells. Gating on the MHC-II$^-$Zbtb46-GFP$^+$population, classical DCs were identified and sorted as CD3ε$^-$TCRβ$^-$ cells, whereas T_DC were identified and sorted as CD3ε$^+$TCRβ$^+$ cells. The three cell types underwent two rounds of sorting to obtain a higher purity as described in [2]. Total RNA was isolated with the RNeasy Micro kit (Qiagen) from 2000 to 3000 cells and then subjected to bulk RNA sequencing.

RNA-seq data processing and analysis

Sequencing Libraries were prepared using SMART Nextera unstranded protocol. Libraries were checked using Qubit (fluorimeter) and Bioanalyzer (capillary electrophoresis). Sequencing was performed using Illumina Nextseq 500 with a HighOutput flow cell, 1 × 75 nt, single read, and Novaseq 6000, 1 × 100 nt, single read. Libraries were found to be of good quality.

FastQC software was used to examine quality of fastq files [33]. Raw sequencing files were trimmed to eliminate adapter sequences, and those trimmed sequences were aligned to the "mm10" mouse genome using STAR aligner (version STAR_2.5.3a) [34, 35] with the featureCounts function was used for counting the abundance of genes. Principal component analysis was performed to evaluate the separation of samples based on decreasing variance. Putative differentially expressed genes were selected using *limma*-voom [36]. The criterion used to select differentially expressed genes in pairwise comparisons is the SEQC cut-off: nominal *p*-value < 0.01 and absolute value of log2 fold change >1 [37].

Single-cell RNA-seq

Raw count datasets from Kiner et al. were downloaded from the Gene Expression Omnibus database under accession no. GSE160055. Specifically, the four datasets corresponding to four infection conditions were analyzed: GSM4859313_SPF, GSM4859314_Citrobacter, GSM4859315_Salmonella, and GSM4859316_Nippo. Single cell data analysis was performed using Seurat (v4.0.1) (Stuart et al., 2019). Note that 6509 cells were obtained after applying the same QC filters used in Kiner et al., that is, cells with less than 1000 UMIs or 400 genes and more than 4000 UMIs or 0.05% of reads mapped to mitochondrial genes were excluded from the analysis.

Moreover, only genes expressed in at least five cells were retained. Samples were merged and the UMI count matrix was further normalized and scaled following the standard Seurat workflow. UMAP reduction was then applied on the first 25 principal components after running PCA.

The plots showing normalized expression values with a color scale on top of UMAP plots and the Violin plot were produced with FeaturePlot and VlnPlot Seurat functions, respectively. The

gene signature average for T_{DC} marker genes was calculated with the AddModuleScore function in Seurat.

Statistical analyses

Flow and imaging data were collected using FlowJo Version 10.5.3 (Treestar) and Imaris (Bitplane), respectively. Statistical analyses were performed with GraphPad Prism software version 9.5 (GraphPad). Results are expressed as mean ± SEM. Means between two groups were compared with unpaired two-tailed *t*-test. Means among three groups were compared with one-way ANOVA. Tukey's posttest was used for multiple comparisons. Significance is indicated as follows: *p value < 0.05; **p value < 0.01; ***p value < 0.001; ****p value < 0.0001. Comparisons are not statistically significant unless indicated.

Conflict of interest: M.I. participates in advisory boards/consultancies for Gilead Sciences, Third Rock Ventures, Asher Biotherapeutics, Clexio Biosciences, Sybilla, and BlueJay Therapeutics.

Author contributions: Conceptualization: M.K. Investigation: A.F., E.S., M.N., V.F., F.O., M.M., and C.C. Resources: M.K. and M.I. Formal analysis: M.K. and A.F. Bioinformatic analysis: C.L., M.R., and P.P. Writing: M.K. with input from all authors. Visualization: M.K. Project supervision: M.K. Funding acquisition: M.K.

Data availability statement: The data that support the findings of this study are openly available in the San Raffaele Open Research Data Repository at: 10.17632/96yb7xc7wh.1. The data that support the findings of the bulk RNA-seq study are openly available in the Gene Expression Omnibus (GEO) database under accession no. GSE237645. The data that support the findings of the comparison between T_{DC} and MyT were derived from the Gene Expression Omnibus (GEO) database under accession no. GSE160055.

Peer review: The peer review history for this article is available at https://publons.com/publon/10.1002/eji.202350529

References

1 **Kuka, M., Munitic, I. and Ashwell, J. D.**, Identification and characterization of polyclonal αβ-T cells with dendritic cell properties. *Nat. Commun.* 2012. **3**: 1223.

2 **Kuka, M. and Ashwell, J. D.**, A method for high purity sorting of rare cell subsets applied to TDC *J. Immunol. Methods* 2013. **400–401**: 111–116.

3 **Eisenbarth, S. C.**, Dendritic cell subsets in T cell programming: location dictates function. *Nat. Rev. Immunol.* 2019. **19**: 89–103.

4 **Qualai, J., Li, L. X., Cantero, J., Tarrats, A., Fernández, M. A., Sumoy, L., Rodolosse, A. et al.**, Expression of CD11c is associated with unconventional activated T cell subsets with high migratory potential. *PLoS One* 2016. **11**: e0154253.

5 **Beyer, M., Wang, H., Peters, N., Doths, S., Koerner-Rettberg, C., Openshaw, P. J. and Schwarze, J.**, The beta2 integrin CD11c distinguishes a subset of cytotoxic pulmonary T cells with potent antiviral effects in vitro and in vivo. *Respir. Res.* 2005. **6**: 70.

6 **Huleatt, J. W. and Lefrançois, L.**, Antigen-driven induction of CD11c on intestinal intraepithelial lymphocytes and CD8+ T cells in vivo. *J. Immunol.* 1995. **154**: 5684–5693.

7 **Lin, Y., Roberts, T. J., Sriram, V., Cho, S. and Brutkiewicz, R. R.**, Myeloid marker expression on antiviral CD8+ T cells following an acute virus infection. *Eur. J. Immunol.* 2003. **33**: 2736–2743.

8 **Satpathy, A. T., KC, W., Albring, J. C., Edelson, B. T., Kretzer, N. M., Bhattacharya, D., Murphy, T. L. et al.**, Zbtb46 expression distinguishes classical dendritic cells and their committed progenitors from other immune lineages. *J. Exp. Med.* 2012. **209**: 1135–1152.

9 **Meredith, M. M., Liu, K., Darrasse-Jeze, G., Kamphorst, A. O., Schreiber, H. A., Guermonprez, P., Idoyaga, J. et al.**, Expression of the zinc finger transcription factor zDC (Zbtb46, Btbd4) defines the classical dendritic cell lineage. *J. Exp. Med.* 2012. **209**: 1153–1165.

10 **Meredith, M. M., Liu, K., Kamphorst, A. O., Idoyaga, J., Yamane, A., Guermonprez, P., Rihn, S. et al.**, Zinc finger transcription factor zDC is a negative regulator required to prevent activation of classical dendritic cells in the steady state. *J. Exp. Med.* 2012. **209**: 1583–1593.

11 **Szklarczyk, D., Kirsch, R., Koutrouli, M., Nastou, K., Mehryary, F., Hachilif, R., Gable, A. L. et al.**, The STRING database in 2023: protein–protein asso

ciation networks and functional enrichment analyses for any sequenced genome of interest. *Nucleic. Acids. Res.* 2023. **51**: D638–D646.

12 **MacDonald, K. P., Rowe, V., Bofinger, H. M., Thomas, R., Sasmono, T., Hume, D. A. and Hill, G. R.**, The colony-stimulating factor 1 receptor is expressed on dendritic cells during differentiation and regulates their expansion. *J. Immunol.* 2005. **175**: 1399–1405.

13 **Mak, K. S., Funnell, A. P., Pearson, R. C. and Crossley, M.**, PU.1 and haematopoietic cell fate: dosage matters. *Int. J. Cell Biol.* 2011. **2011**: 808524.

14 **Miller, J. C., Brown, B. D., Shay, T., Gautier, E. L., Jojic, V., Cohain, A., Pandey, G. et al.**, Deciphering the transcriptional network of the dendritic cell lineage. *Nat. Immunol.* 2012. **13**: 888–899.

15 **Subramanian, A., Tamayo, P., Mootha, V. K., Mukherjee, S., Ebert, B. L., Gillette, M. A., Paulovich, A. et al.**, Gene set enrichment analysis: a knowledge-based approach for interpreting genome-wide expression profiles. *Proc. Natl. Acad. Sci. USA* 2005. **102**: 15545–15550.

16 **Franzén, O., Gan, L.-M. and Björkegren, J. L. M.**, PanglaoDB: a web server for exploration of mouse and human single-cell RNA sequencing data. *Database* 2019. **2019**.https://doi.org/10.1093/database/baz046

17 **Mouchacca, P., Schmitt-Verhulst, A. M. and Boyer, C.**, Visualization of cytolytic T cell differentiation and granule exocytosis with T cells from mice expressing active fluorescent granzyme B. *PLoS One* 2013. **8**: e67239.

18 **Chiu, C. and Openshaw, P. J.**, Antiviral B cell and T cell immunity in the lungs. *Nat. Immunol.* 2015. **16**: 18–26.

19 **Heymann, F. and Tacke, F.**, Immunology in the liver — from homeostasis to disease. *Nat. Rev. Gastroenterol. Hepatol.* 2016. **13**: 88–110.

20 **Ficht, X. and Iannacone, M.**, Immune surveillance of the liver by T cells. *Sci. Immunol.* 2020. **5**: eaba2351.

21 **Zinkernagel, R. O. L. F. M., Haenseler, E., Leist, T. H. O. M. A. S., Cerny, A. N. D. R. E. A. S., Hengartner, H. A. N. S. and Althage, A. L. A. N. A.**, T cell-mediated hepatitis in mice infected with lymphocytic choriomeningitis virus. Liver cell destruction by H-2 class I-restricted virus-specific cytotoxic T cells as a physiological correlate of the 51Cr-release assay? *J. Exp. Med.* 1986. **164**: 1075–1092.

22 **Kiner, E., Willie, E., Vijaykumar, B., Chowdhary, K., Schmutz, H., Chandler, J., Schnell, A. et al.**, Gut CD4+ T cell phenotypes are a continuum molded by microbes, not by TH archetypes. *Nat. Immunol.* 2021. **22**: 216–228.

23 **McGinnis, C. S., Murrow, L. M. and Gartner, Z. J.**, DoubletFinder: doublet detection in single-cell RNA sequencing data using artificial nearest neighbors. *Cell Syst.* 2019. **8**: 329–337.e4.

24 **Kastenmuller, W., Torabi-Parizi, P., Subramanian, N., Lammermann, T. and Germain, R. N.**, A spatially-organized multicellular innate immune response in lymph nodes limits systemic pathogen spread. *Cell* 2012. **150**: 1235–1248.

25 **Zhou, W., Zhou, L., Zhou, J., JRI, L. C. B., Chu, C., Zhang, C., Sockolow, R. E. et al.**, *Nature* 2022. **609**: 159–165.

26 **Liang, K. L., Roels, J., Lavaert, M., Putteman, T., Boehme, L., Tilleman, L., Velghe, I. et al.**, Intrathymic dendritic cell-biased precursors promote human T cell lineage specification through IRF8-driven transmembrane TNF. *Nat. Immunol.* 2023. **24**: 474–486.

27 **Pallett, L. J., Swadling, L., Diniz, M., Maini, A. A., Schwabenland, M., Gasull, A. D., Davies, J. et al.**, *Nature* 2023. **614**: 334–342.

28 **Mouchacca, P., Guyot, V., Gregoire, C., Schmitt-Verhulst, A. M. and Boyer, C.**, Granzyme B-tdTomato, a new probe to visualize cytolytic effector cell activation. *Eur. J. Immunol.* 2012. **42**: 264–266.

29 **Welsh, R. M. and Seedhom, M. O.**, *Curr Protoc Microbiol* 2008. **Chapter 15**: Unit 15A.1. No pages numbers. PMID: 18770534

30 **Sammicheli, S., Kuka, M., Di Lucia, P., de Oya, N. J., De Giovanni, M., Fioravanti, J., Cristofani, C. et al.**, Inflammatory monocytes hinder antiviral B cell responses. *Sci. Immunol.* 2016. **1**.

31 **Cossarizza, A., Chang, H. D., Radbruch, A., Abrignani, S., Addo, R., Akdis, M., Andrä, I. et al.**, Guidelines for the use of flow cytometry and cell sorting in immunological studies (third edition). *Eur. J. Immunol.* 2021. **51**: 2708–3145.

32 **De Giovanni, M., Cutillo, V., Giladi, A., Sala, E., Maganuco, C. G., Medaglia, C., Di Lucia, P. et al.**, Spatiotemporal regulation of type I interferon expression determines the antiviral polarization of CD4+ T cells. *Nat. Immunol.* 2020. **21**: 321–330.

33 **Andrews, S.**, FastQC: a quality control tool for high throughput sequence data. 2010. http://www.bioinformatics.babraham.ac.uk/projects/fastqc

34 **Dobin, A., Davis, C. A., Schlesinger, F., Drenkow, J., Zaleski, C., Jha, S., Batut, P. et al.**, STAR: ultrafast universal RNA-seq aligner. *Bioinformatics* 2013. **29**: 15–21.

35 **Liao, Y., Smyth, G. K. and Shi, W.**, The R package Rsubread is easier, faster, cheaper and better for alignment and quantification of RNA sequencing reads. *Nucleic Acids Res.* 2019. **47**: e47–e47.

36 **Ritchie, M. E., Phipson, B., Wu, D. I., Hu, Y., Law, C. W., Shi, W. and Smyth, G. K.**, limma powers differential expression analyses for RNA-sequencing and microarray studies. *Nucleic Acids Res.* 2015. **43**: e47–e47.

37 **Consortium, S. E. Q. C.-I. I. I.**, A comprehensive assessment of RNA-seq accuracy, reproducibility and information content by the Sequencing Quality Control Consortium. *Nat. Biotechnol.* 2014. **32**: 903–914.

38 **Shannon, P., Markiel, A., Ozier, O., Baliga, N. S., Wang, J. T., Ramage, D., Amin, N. et al.**, Cytoscape: a software environment for integrated models of biomolecular interaction networks. *Genome Res.* 2003. **13**: 2498–2504.

Abbreviations: **LCMV**: lymphocytic choriomeningitis virus

Full correspondence: Dr. Mirela Kuka, School of Medicine, Vita-Salute San Raffaele University, Milan, Italy
e-mail: kuka.mirela@hsr.it